Struct Multidisc Optim (2010) 41:163–177
DOI 10.1007/s00158-009-0416-y

RESEARCH PAPER

A topology optimization method for design of negative permeability metamaterials

Alejandro R. Diaz · Ole Sigmund

Received: 11 March 2009 / Revised: 13 May 2009 / Accepted: 11 June 2009 / Published online: 16 July 2009

Abstract A methodology based on topology optimization for the design of metamaterials with negative permeability is presented. The formulation is based on the design of a thin layer of copper printed on a dielectric, rectangular plate of fixed dimensions. An effective media theory is used to estimate the effective permeability, obtained after solving Maxwell's equations on a representative cell of a periodic arrangement using a full 3D finite element model. The effective permeability depends on the layout of copper, and the subject of the topology optimization problem is to find layouts that result in negative (real) permeability at a prescribed frequency. A SIMP-like model is invoked to represent the conductivity of regions of intermediate density. A number of different filtering strategies are invoked to facilitate convergence to binary solutions. Examples of designs for S-band applications are presented for illustration. New metamaterial concepts are uncovered, beyond the classical split-ring inspired layouts.

Keywords Metamaterials · Negative permeability · Topology optimization

A. R. Diaz (✉)
Mechanical Engineering, Michigan State University,
East Lansing, MI 48824, USA
e-mail: diaz@egr.msu.edu

O. Sigmund
Department of Mechanical Engineering, Section for Solid Mechanics,
Technical University of Denmark, DK-2800 Lyngby, Denmark
e-mail: sigmund@mek.dtu.dk

1 Background: the split ring resonators

Since the re-discovery in 2000 (Pendry 2000; Smith et al. 2000) of double negative materials—as earlier described in a paper by Veselago (1968)—there has been a rush to find realizations of negative index materials or, more generally, electromagnetic metamaterials. These are engineered materials that exhibit exceptional properties that are not observed in the constituents and result from the inclusion of artificially fabricated inhomogeneities. Most electromagnetic metamaterials are realized as small structures of dielectric or metallic inclusions in a host substrate, repeated periodically in arrays of identical cells. The size of the small structures varies depending on the application, from sub-mm for optical to a few millimeters in radio-frequency (RF) applications. In the case of metamaterials with negative permeability, most realizations to date have been based on variations of the so-called split ring resonator (SRR) arrangement (Fig. 1a). Split ring resonators, now widely discussed in the literature, were popularized after the publication of Pendry et al. (1999), although loops loaded with capacitance were used as early as the 1950s as a mechanism to modify the permeability of artificial dielectrics (Schelkunoff and Friis 1952). In the SRR design—as is the case in essentially all other designs discussed in the literature—the geometric arrangement of the conducting material (the "split ring") on the substrate is determined in a somewhat ad-hoc fashion. In this work we present a more general strategy, based on topology optimization.

Most naturally occurring materials are so-called "double positive", i.e., materials with positive real permittivity and permeability. Pendry et al. (1999) showed that copper SRRs printed in periodic arrangements on a dielectric backing plate behave as a homogeneous material having negative effective permeability. By adjusting the dimensions and

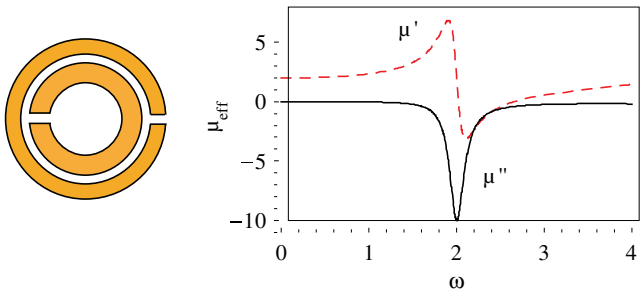

(a) (b)

Fig. 1 A typical SRR (**a**) and a typical effective permeability curve (**b**)

other details of the rings (radii, gap size), the authors made the SRR resonant, leading to a negative effective permeability in a region near the high frequency side of the resonance (Fig. 1b). The periodic arrangement of the resonators results in strong magnetic coupling of the units and an effective permeability μ_{eff} which can be approximated by the expression

$$\mu_{eff}(\omega) = \mu'(\omega) + j\mu''(\omega) = 1 - \frac{F\omega^2}{\omega^2 - \omega_0^2 + j\omega\Gamma} \quad (1)$$

In (1) μ_{eff} is a complex function of the frequency of incident radiation ω, with real part μ' and imaginary part μ''. Expressions for Γ, F and ω_0 as functions of material and geometric parameters are given in Pendry et al. (1999) and Smith et al. (2000). Similar expressions for μ_{eff} have been derived by a number of authors for resonators of different geometries based on LC circuit analogies (Marqués et al. 2008). Note that in this paper we show the effective permeability with *negative* imaginary part. Depending on educational background, other authors may use a different sign convention, leading to a positive μ''. Here a negative imaginary part μ'' implies that material damping is measured as a negative imaginary part of the material parameters.

In RF applications a SRR design can be implemented using printed circuit board technology and readily available sheets of copper-coated dielectric plates. The SRR pattern is easily "printed" on the plate using either chemical or mechanical means. The same technique can be used to print more complicated patterns. The analysis leading to the computation of an effective permeability must rely on a suitable effective media theory. This typically requires the full solution of Maxwell's equations on the 3D representative cell containing the copper-coated plates. Several effective media theories have been proposed in the literature (e.g., Smith et al. 2005; Lerat et al. 2006; Smith and Pendry 2006) and can be used in this context. Depending on the shape of the small copper structures, $\mu_{eff}(\omega)$ *may* exhibit resonant behavior of the type reported in Fig. 1 for the SRR.

There are many reasons why one would want to explore alternative arrangements of small structures of conductive material, including reduced losses, broadband response and the potential to achieve simultaneously negative permeability and permittivity. As we will show in the sequel, many geometries result in resonant behavior. Unfortunately, they are quite difficult to find and finding them requires the application of a specially tailored design methodology. This work explores formulations of the topology optimization problem that result in new metamaterial concepts with negative permeability and uncover new designs, beyond the classical split-ring inspired layouts.

2 Analysis and effective properties

We consider a periodic arrangement of inclusions characterized by 3D cells. Each cell is a parallelepiped with a centrally located inclusion, as shown in Fig. 2a. The inclusions are thin rectangular plates made of a lossless homogeneous dielectric. A thin layer of copper, symmetric about the (horizontal) y_1 axis, is printed on one face of each plate, as shown in Fig. 2a. To ensure invariance to waves propagating in the positive or negative y_1 direction, the same layout, rotated 180° about the vertical y_2 axis, is printed on the opposite face (see Fig. 2a). The cells are illuminated by a transversely polarized, uniform incident plane wave $\mathbf{E}^i = \mathbf{E}^0 e^{-jk\mathbf{k}\cdot\mathbf{r}}$[1] with propagation direction $\mathbf{k}$ normal to one of the cell faces and parallel to the plane of the inclusion. To simplify computations we consider only perpendicular radiation, leaving the more general problem of arbitrarily oriented excitation for further studies.

A *metasurface* is built from an infinitely periodic tiling of these cells with tiling vectors along the incident $\mathbf{E}$ and $\mathbf{H}$ directions (Fig. 2b). When the wavelength λ of the dominant mode propagating through the metasurface is sufficiently large—typically $\lambda > 10d$, where d is the characteristic length of the cell—the metasurface behaves as a homogeneous slab of effective properties $\varepsilon_{eff}(\omega)$ and $\mu_{eff}(\omega)$. It should be emphasized that, as the slab is only one cell deep, one should be careful in interpreting the meaning of these properties. Effective properties can change drastically as the number of cells in the thickness direction increases, as discussed in Rockstuhl et al. (2008). Our computations are valid for one layer slabs and an incoming radiation that is perpendicular to the slab and it is only in that restricted context that we refer to $\varepsilon_{eff}(\omega)$ and $\mu_{eff}(\omega)$ as the "effective properties".

[1] As usual, the frequency dependent factor $e^{j\omega t}$ is omitted.

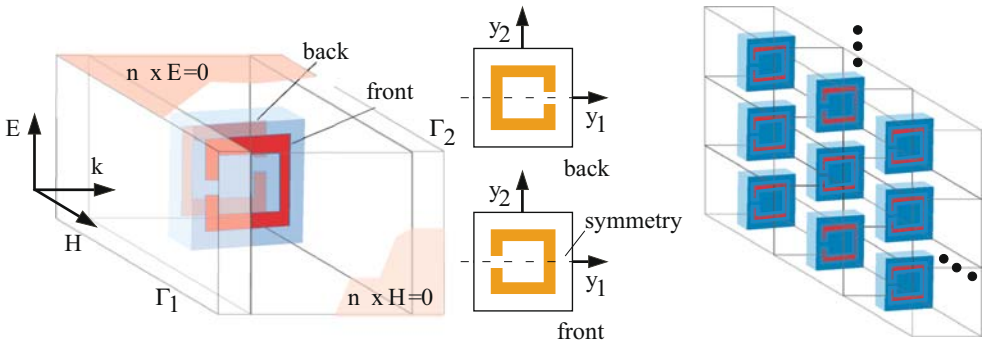

(a) (b)

Fig. 2 A representative cell (**a**) and a metasurface (**b**) in the present metamaterial design problem

2.1 Analysis

Several effective media theories have been postulated to compute the effective properties $\varepsilon_{eff}(\omega)$ and $\mu_{eff}(\omega)$ of the slab from the solution of Maxwell's equations on a single cell Ω,

$$\nabla \times \left(\frac{1}{\mu_r}\nabla \times \mathbf{E}\right) + \left(\varepsilon_r - j\frac{\sigma}{\omega\varepsilon_0}\right)\mathbf{E} = 0 \text{ in } \Omega \tag{2a}$$

expressed in terms of the electric field $\mathbf{E}$. In (2a), ε_r, μ_r and σ are, respectively, the relative permittivity and permeability and the conductivity of the medium in Ω and ε_0 is the free space permittivity. Under the symmetry assumptions imposed on the material distribution and for an incident field propagating in a direction normal to a cell face, as shown in Fig. 2a, boundary conditions

$$\mathbf{n} \times \mathbf{E} = 0 \text{ on } \Gamma_E \quad \text{and} \quad \mathbf{n} \times \mathbf{H} = 0 \text{ on } \Gamma_H \tag{2b}$$

are used to enforce periodicity on the faces Γ_E and Γ_H, respectively normal to the incident $\mathbf{E}$ and $\mathbf{H}$ vectors. Note that a small approximation is made here, since the material distribution is not exactly symmetric about the y_1-y_2 plane (compared to the front plane layer, the layer printed on the back plane is rotated 180° about the vertical axis). However, assuming that the thickness of the plate is much smaller than the cell width, the field can be considered symmetric about the y_1-y_2-plane and hence the periodicity boundary conditions can be substituted by the simpler boundary conditions (2b).

As inlet and outlet conditions we use the scattering boundary conditions (2c) and (2d) below. These are first order boundary conditions, and assume that the waves are propagating perpendicularly to the corresponding input and output boundaries Γ_1 and Γ_2. These conditions are commonly used in the literature in the context of S-parameter extraction methods (Jin 2002) Even though this is a rather crude assumption, we do not expect that other boundary conditions will change the resulting design significantly. Under these assumptions, the incident field $\mathbf{E}^i$ results in boundary conditions

$$\mathbf{n} \times (\nabla \times \mathbf{E}) - jk_0\mathbf{n} \times (\mathbf{E} \times \mathbf{n}) = -2jk_0\mathbf{E}^i \text{ on } \Gamma_1 \tag{2c}$$

and

$$\mathbf{n} \times (\nabla \times \mathbf{E}) - jk_0\mathbf{n} \times (\mathbf{E} \times \mathbf{n}) = 0 \text{ on } \Gamma_2 \tag{2d}$$

Γ_1 and Γ_2 are, respectively, the input and output surfaces, k_0 is the free space propagation constant and $\mathbf{n}$ is the vector normal to the corresponding surface (Fig. 2a). Note that inlet and outlet regions separate the inclusion from the boundaries Γ_1 and Γ_2. Equations (2a), (2b), (2c), and (2d) are solved using a finite element discretization of Ω (Fig. 3).

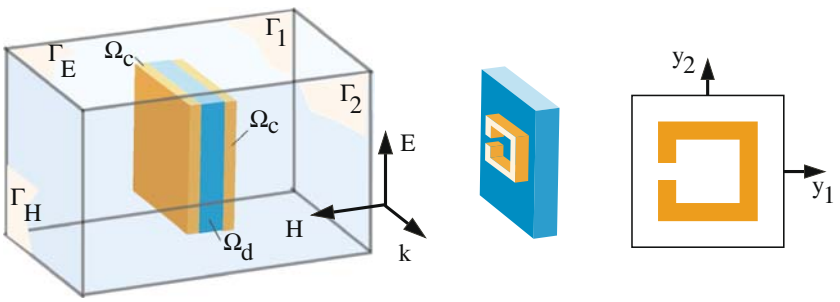

(a) (b) (c)

Fig. 3 The subdomains Ω_d, Ω_c, Ω_0 of the representative cell Ω (**a**). The conductive layer is in Ω_c (**b**) and can be represented using a 2D layout, symmetric about the y_1 axis (**c**)

Three separate sub-domains of Ω with different material properties are identified:

Ω_d: the backing plate. Here the material is a perfect dielectric with relative permittivity $\varepsilon_r = \varepsilon_d$ and permeability $\mu_r = 1$.

Ω_c: a thin layer on either side of Ω_d on which the conductive material is printed. Conductivity at a point $\mathbf{x} \in \Omega_c$ is that of either copper or void.

Ω_0: the (void) space in Ω that is not Ω_d or Ω_c. A small space is kept between the edges of the inclusion and the exterior faces of Ω in the $\pm\,\mathbf{k}$ directions. Thus the input and output surfaces Γ_1 and Γ_2 are some distance away from the inclusion.

In the next section we define the goal of the optimization problem as one of finding the distribution of conductive material in Ω_c, i.e., the shape of the copper layer.

2.2 Effective properties

A number of effective media theories can be used to compute effective properties from the solution $\mathbf{E}$ of (2a), (2b), (2c), and (2d). Here we use the model proposed by Smith et al. (2005), which works well for periodic arrangements that are one-cell deep in the $\mathbf{k}$ direction. Computation of effective properties requires that the S parameters be calculated first. For this problem the S parameters are obtained from the formulas

$$S_{11} = \frac{\int\limits_{\Gamma_1} \left(\mathbf{E} - \mathbf{E}^i\right) \cdot \mathbf{E}^i d\Gamma}{\int\limits_{\Gamma_1} \mathbf{E}^i d\Gamma} \tag{3}$$

$$S_{21} = \frac{\int\limits_{\Gamma_2} \mathbf{E} \cdot \mathbf{E}^i d\Gamma}{\int\limits_{\Gamma_1} \mathbf{E}^i d\Gamma} \tag{4}$$

Once the S parameters are computed, estimates of $\mu_{eff}(\omega)$ can be computed from

$$\mu_{eff} = \frac{Z \cos^{-1}\left(\beta / \left(2S_{21}\right)\right)}{2\pi} \left(\lambda / d\right) \tag{5}$$

where

$$\beta = 1 - S_{11}^2 + S_{21}^2 \tag{6}$$

and

$$Z^2 = \frac{2 + 2S_{11} - \beta}{2 - 2S_{11} - \beta} \tag{7}$$

3 Optimization problem

3.1 Selection of the design variable

The effective permeability of the slab depends on the layout of conductive material in each cell. As the conductive layer is "printed" as a thin layer in Ω_c, its layout can be characterized by the 2D indicator function

$$\chi(\mathbf{y}) = \begin{cases} 1 & \text{if} \quad \sigma(\mathbf{y}) = \sigma_c \\ 0 & \text{if} \quad \sigma(\mathbf{y}) = 0 \end{cases} \tag{8}$$

and the associated, unique inverse relation $\sigma(\mathbf{y}) = \chi(\mathbf{y})^* \sigma_c$. In (8) σ_c is the conductivity of the conductive layer (e.g., the conductivity of copper, $\sigma_c = 5.8 * 10^7$ (s/m)) and $\mathbf{y} \in D = [0, a] \times [0, b]$ for an $a \times b$ rectangular backing plate. Thus, at least formally, the topology optimization problem is cast in its classical material design form, where the goal is to find an indicator function χ that controls the layout of material 1 (copper, high conductivity) in a background of material 2 (void, non conductive). The design domain is the region D.

A SIMP-like model (Bendsøe 1990; Rozvany et al. 1992; Mlejnik and Schirrmacher 1993) is invoked to assign conductivity values to regions of intermediate density. $\chi(\mathbf{y})$ is replaced by $\rho(\mathbf{y})$ which varies continuously in [0,1]. Further, $\rho(\mathbf{y})$ is piece-wise constant, taking constant values $\{\rho_1, \rho_2, \ldots, \rho_N\}$ over regular subsets of D—sometimes referred to as "pixels"—in a discretization consistent with the finite element model. As the indicator function χ is replaced by ρ, special care must be exercised in the selection of the interpolation scheme that assigns conductivity values to points of intermediate density $0 < \rho < 1$. This is a delicate step in the present problem, as the magnitude of the conductivity σ_c at $\chi = 1$ has a strong effect on the solution, and thus the *range* of values of σ in the design domain is crucial. This is in sharp contrast with standard topology optimization problems in elasticity, where solutions can be scaled so that the *magnitude* of the elastic modulus at $\chi = 1$ is not relevant.

To facilitate the definition of an appropriate interpolation scheme it is useful to express the conductivity in logarithmic scale, defining first the interpolation scheme using

$$\sigma_{dB}(\rho) = \sigma_{dB}^H - \frac{1 - \rho}{1 + \rho}\left(\sigma_{dB}^H - \sigma_{dB}^L\right) \tag{9a}$$

and

$$\sigma(\rho) = 10^{\sigma_{dB}} \tag{9b}$$

where the conductivity in log scale σ_{dB} has range $\left[\sigma_{dB}^L, \sigma_{dB}^H\right]$. Expressing $\sigma(\rho)$ as an exponential function of ρ guarantees that the conductivity decays rapidly away from

$\rho = 1$. The upper bound σ_{dB}^{H} is set to correspond to the property of the conductive material: for copper,

$$\sigma_{dB}^{H} = \log_{10}(\sigma_{Cu}) = \log_{10}\left(5.8{*}10^{7}\right) \approx 7.8$$

The lower bound σ_{dB}^{L} can be adjusted to control the rate of change of σ in log scale, which is proportional to $\left(\sigma_{dB}^{H} - \sigma_{dB}^{L}\right)$. σ_{dB}^{L} should be small enough so that $\rho = 0$ simulates a non-conductive material. Numerical experiments suggest that σ_{dB}^{L} values of -5 to -7 guarantee that $\sigma(0)$ is sufficiently small while still allowing small changes in ρ to have a measurable effect on σ, even in the lower end of the ρ scale. Figure 4 shows the functions $\sigma_{dB}(\rho)$ and $\sigma(\rho)$ for different values of σ_{dB}^{L}.

3.2 Objective function and constraints

A negative effective property—permeability or permittivity—is the result of a resonance phenomenon. To illustrate using the simple model in (1), a region of negative μ' at a target frequency Ω^0 appears when there is a resonance ω_0 at a frequency near Ω^0. Naturally, when negative permeability is the goal, one would then look for designs that have a resonant frequency in this neighborhood, and thus using $\mu'(\Omega^0)$ or $\mu''(\Omega^0)$ as the objective function should result in $\mu' < 0$ near Ω^0. We use $\mu''(\Omega^0)$ as the objective function in the following optimization problem:

For a given frequency Ω^0, find $\rho = \{\rho_1, \rho_2, \ldots, \rho_N\}$ that:

$$\begin{aligned} &\text{minimizes} \quad \Phi(\rho) = \mu''\left(\Omega^0\right) \\ &\text{subject to} \quad 0 \le \rho_e \le 1,\ e = 1, 2 \ldots, N \end{aligned} \tag{10}$$

While other formulations of the problem are possible, our experience has been that this particular choice of objective function leads to more efficient computations. Indeed, minimization of μ'' is preferable to μ' from a computational point of view simply because of the non-convex nature of the function $\mu'(\omega)$. Approaching a solution from the "wrong side" of the resonance, the direction of increasing $\mu'(\omega)$, will lead to failure of most standard gradient-based algorithms. However, with some care, μ' may be used as the objective function also, provided that a suitable initial design is found, as illustrated later in one of the solved examples. Furthermore, except for the simple bounds on the design variables, problem (10) is essentially unconstrained and this also results in better performance in computations. Using μ'' as the objective and the absence of constraints allow for the use the standard arsenal of gradient-based algorithms that are typical in topology optimization. Finally, optimization over a range of frequencies, e.g., to affect bandwidth, would also be of practical interest, but is beyond the scope of this work and is left for future investigations.

Analysis is performed using finite elements. N is the number of element faces on $D = [0, a] \times [0, b]$, the rectangular *surface* on one side of Ω_c. Bounds on the total amount of each constituent are not necessary in this case: the "strongest" resonance does not call for the use of only one phase.

In the sequel we will show that problem (10) has many local solutions but finding *binary* solutions is particularly difficult and in many ways different from classical topology optimization problems.

3.3 Shape control, processing and post-processing

One of the most difficult aspects of this problem involves controlling the outcome of the solution of problem (10) to guarantee a binary ($\rho_e \in \{0, 1\}$, i.e., "black-white") solution. To illustrate the difficulties associated with this problem it may be useful to introduce a simple mechanical analogy. We use three linear springs connected in series, as shown in Fig. 5a, and the spring stiffnesses (k_1, k_2) as design variables. The behavior of the system under a periodic load F is modeled by the equations $\left(K - \omega^2 M\right) U = F$ where ω is the frequency of excitation and

$$K = \begin{pmatrix} k_1 + k_2 & -k_2 \\ -k_2 & 1 + k_2 \end{pmatrix} \quad \text{and} \quad M = \begin{pmatrix} 1 & 0 \\ 0 & 1 \end{pmatrix}$$

If we only look at the first (lower) mode of vibration of this system, the *amplitude* of the modal response is

$$A(k_1, k_2, \omega) = \frac{1}{\omega_0^2(k_1, k_2) - \omega^2 + j\zeta\omega} \tag{11}$$

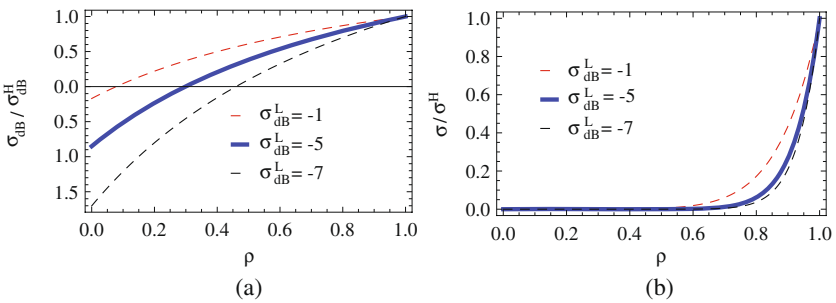

Fig. 4 Conductivity σ as a function of effective density ρ in log-scale (**a**) and linear scale (**b**)

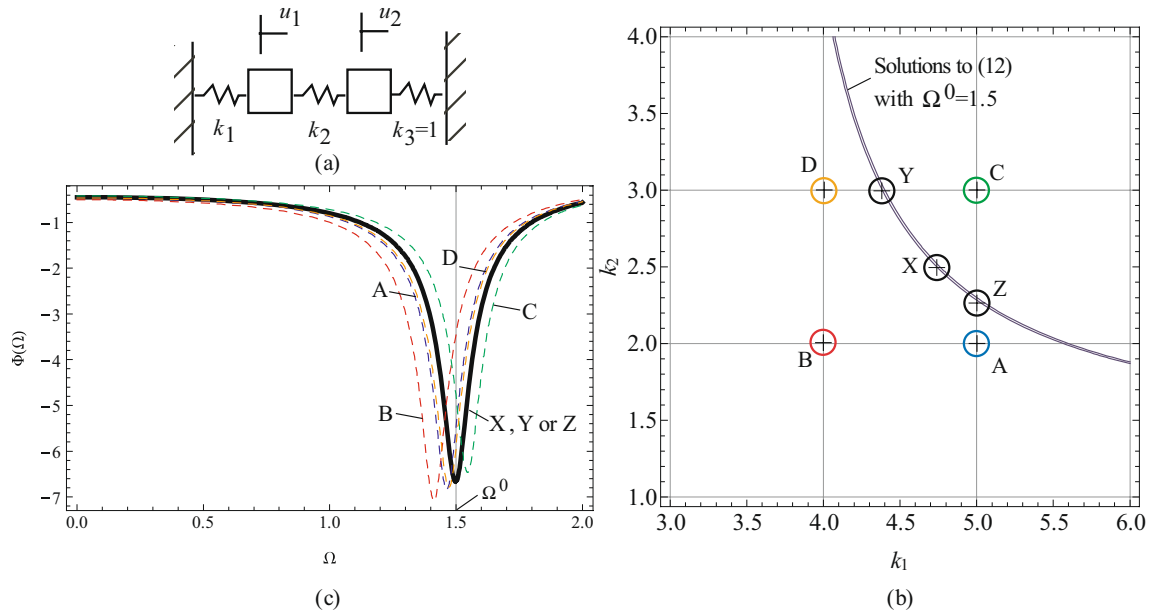

Fig. 5 Mechanical analogy of the metamaterial design optimization problem. (**a**) The system. (**b**) The locus of solutions to (12) with $\Omega^0 = 1.5$. Designs X Y and Z are all local optima. (**c**) Frequency response of locally optimal solutions (X, Y or Z) and of non-optimal, neighboring designs with integer spring constants (A, B, C or D)

(after adding a small amount of constant damping ζ) which, as is well known, has a resonance when the driving frequency ω is near ω_0, the first natural frequency of the system. ω_0^2 is the lowest eigenvalue of K and thus ω_0: $\omega_0 (k_1, k_2)$. The amplitude function A is qualitatively similar to the effective permeability function μ (see (1)), where now the spring parameters (k_1, k_2) play the role of the effective densities ρ_e. The optimization problem (10) is qualitatively similar to finding solutions to the problem

$$\min_{k_1,k_2} \Phi(k_1, k_2) = -|A(k_1, k_2, \Omega_0)| \tag{12}$$

which, simply stated, seeks to find the spring values that result in the largest possible amplitude at a given driving frequency Ω_0.

Solutions to (12) occur at points (k_1^*, k_2^*) such that $\omega_0(k_1^*, k_2^*) = \Omega^0$, i.e., when the springs are selected such that the first natural frequency coincides with the (prescribed) driving frequency Ω^0. These solutions are, in general, not unique, as we know that there could be many spring values that result in the same first natural frequency. However, the condition $\omega_0(k_1, k_2) = \Omega^0$ which characterizes solutions to (12) may never be met if we demand that (k_1, k_2) take only integer values. *This is precisely what we do when we require that variable ρ representing the distribution of conductive material be binary*.

In topology optimization, when convergence to binary solutions is not achieved naturally, the standard approach is to 'coax' solutions towards near-binary results using filters or similar artifices. While never *guaranteeing* a fully binary solution, these methods result in near-binary solutions from which the few "gray" areas left are easily removed by applying a simple threshold. In our spring analogy, this may mean that through filters we may converge to answers Y or Z instead of X in Fig. 5b. From there, a near-by integer solution can be selected, e.g., points labeled A, B, C, or D in the figure. In topology optimization problems such as minimum compliance, the final threshold step can be applied without affecting performance: removal of a few gray pixels will not affect a global performance measure such as mean compliance. Unfortunately, this is not the case in the metamaterial problem. Removal of even a small number of gray pixels can shift the location of the resonance and change performance substantially. In the spring example this behavior is illustrated in Fig. 5c, which compares the response of the "gray" local optimum (X) to that of the near-by integers solutions, (A, B, C, or D). The magnitude of the response amplitude at Ω^0 deteriorates significantly, dropping from 6.67 for solution (B) to as low as 3.43 for solution (D).

The simple spring example illustrates some of the difficulties associated with the solution of (10). In summary:

1. There are many locally optimal solutions to the metamaterial design problem (10). Thus, even when a binary solution to problem (10) is known to exist, finding it using standard gradient based schemes is difficult.

Convergence to a *particular* solution is strongly dependent on the initial conditions of the search algorithm.

2. For fixed cell dimensions, material properties and discretization of $\rho(\mathbf{y})$, existence of a *binary* solution with a resonance at a *prescribed* frequency Ω^0 is not guaranteed.
3. Since performance is evaluated at a point of resonance, removing even a small amount of "gray" from an otherwise mostly binary design can shift the point of resonance and result in a very significant change in the objective function.

We leave the spring example with a final observation. As discussed above, solutions $\left(k_1^*, k_2^*\right)$ to $\max_{k_1,k_2} A\left(k_1, k_2, \Omega\right)$ occur when $\omega_0\left(k_1^*, k_2^*\right) = \Omega^0$. If the spring stiffness are fixed at these values, the solution to $\max_{\omega} A\left(k_1^*, k_2^*, \omega\right)$ occurs at $\omega^{*2} = \omega_0^2\left(k_1^*, k_2^*\right) - \frac{1}{2}\zeta^2$ and hence $\omega^{*2} = \Omega^{02} - \frac{1}{2}\zeta^2$. It follows that $\omega^* \neq \Omega^0$ unless there is no damping. Thus, the solution to (12)—minimization over *design* at a fixed driving frequency—will not result in the largest amplitude over all frequencies—minimization over *frequencies* ω at a fixed design. This will be true also in the metamaterial design problem.

3.4 Modification of material properties: continuation strategies and filtering

A number of different filtering strategies may be invoked to *facilitate* convergence to "near-binary" solutions with a resonance at a prescribed frequency. A combination of standard filters and a continuation scheme applied to the material model are used here.

Morphology filters, as defined by Guest et al. (2004) and Sigmund (2007), and designed to remove gray regions, do not seem to perform very well in this problem. Of the filters reported in Sigmund (2007), the more successful in this problem are the standard filters introduced by Bruns and Tortorelli (2001) and Bourdin (2001). However, these filters control feature size by averaging properties over several pixels, and thus they introduce small gray areas at the 1–0 (black–white) interfaces. To minimize the effect of these small gray regions, we use a continuation scheme.

The continuation scheme used is similar to increasing the penalization parameter in the standard SIMP material model discussed, e.g., in Bendsøe (1990), Rozvany et al. (1992), and Mlejnik and Schirrmacher (1993), and is designed to mimic a threshold operation around $\rho = 0.5$ as the continuation parameter increases. We used the function

$$f_p(\rho) = \frac{1}{2} + \frac{\tan^{-1}\left(p\left(2\rho - 1\right)\right)}{2\tan^{-1}\left(p\right)} \tag{13}$$

(Fig. 6) where p is the continuation parameter. f_p is applied on both sides of the filter.

The final mapping between the design variable ρ and the material property σ is then:

$$\sigma\left(\rho\right) = 10^{\sigma_{dB}} \tag{14a}$$

where

$$\sigma_{dB} = \sigma_{dB}^H - \frac{1-\rho^F}{1+\rho^F}\left(\sigma_{dB}^H - \sigma_{dB}^L\right) \tag{14b}$$

and the *filtered* density ρ^F is:

$$\rho^F = \left(f_p \circ f_{filter} \circ f_p\right)\rho \tag{14c}$$

f_{filter} represents the filter operation, typically the standard filters reported in Bruns and Tortorelli (2001) and Bourdin (2001). The filtered variable ρ^F is the material variable.

3.5 Sensitivity analysis

Sensitivity analysis in this problem is standard. Two adjoint problems must be solved, one each to compute the gradients of the S parameters S_{11} and S_{21} in (3) and (4). These problems can be represented by equations of the general form

$$K\lambda^{ij} = \frac{\partial S_{ij}}{\partial E}, \quad \frac{\partial S_{ij}}{\partial \rho^F} = \left(\lambda^{ij}\right)^t P \quad \text{and} \quad P = -\frac{\partial K}{\partial \rho^F}E$$

where it has been assumed that the discretized form of Maxwell's equations on Ω is of the form $KE = F$ and F is design independent. The only notable issue here is the complexity of the computation of the pseudo-load vector P. This computation is simplified significantly using the technique described in Olesen et al. (2006). Once values for $\frac{\partial S_{11}}{\partial \rho^F}$ and $\frac{\partial S_{21}}{\partial \rho^F}$ are computed, computation of $\frac{\partial \mu'}{\partial \rho}$ and $\frac{\partial \mu''}{\partial \rho}$ requires

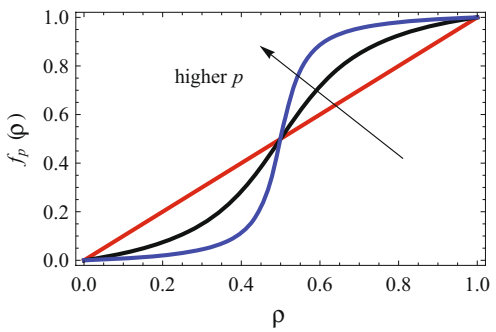

Fig. 6 Function f_p in (13) used to build the material model

only simple algebra and careful application of the chain-rule using (14a) and (14b).

3.6 Algorithm

Recall from the earlier discussion that problem (10) has many local optima. The solution algorithm is organized in three stages, designed to navigate the complex design topography that arises from these local solutions. In the first stage we apply filters to find solutions close to a local optimum that meet simple shape restrictions. In the second stage the solution is refined with filters removed. In the last stage, thresholds are applied and near-by binary solutions are reported.

In stage 1 of the algorithm we seek to get close to solutions that meet feature size restrictions that can be imposed through filters. A standard filter is used (Bruns and Tortorelli 2001; Bourdin 2001) with a prescribed influence radius r_{max}. The continuation scheme with parameter p in (14a) and (14b) is updated according to the following rule:

```
if mod (iter, 10) = 0 and Φ(ρ) ≤ Φ^(p)
    if p < 2
        p = 2.2*p
    else
        p = min(pmax, p + 1)
    end
    Φ^(p) = Φ(ρ)
end
```

starting from $\rho = 0.1$ and $\Phi^{(0.1)} = \infty$. A gradient-based method (Svanberg's MMA algorithm, Svanberg (1987)) with iteration counter *iter* is used, stopping after a fixed number of iterations (40 is typical) or when no further change is detected. The procedure may be re-started from the last *filtered* density ρ^F to remove excessive drift between ρ and ρ^F.

The solution found after the first stage is refined in stage 2 to find a solution that satisfies first order optimality conditions. Again a gradient-based method is used (Svanberg 1987), starting from the best ρ^F from stage 1. No filters or continuation parameters are used in this stage. However, only the remaining gray pixels are used as design variables. Iterations stop when first order necessary conditions are satisfied or a maximum number of iterations is exceeded. For problem (10), first order necessary conditions are

$$\frac{\partial \Phi}{\partial \rho_i} = \begin{cases} \eta_i > 0 & \text{if} \quad \rho_i = 0 \\ \eta_i = 0 & \text{if} \quad 0 < \rho_i < 1 \\ \eta_i < 0 & \text{if} \quad \rho_i = 1 \end{cases} \tag{15}$$

In the final stage, a simple threshold is applied to remove any remaining gray pixels.

4 Examples

We present as the test examples the design of a metamaterial with negative permeability to be used in an S-band application. The goal is to find a material layout that results in a resonance in the neighborhood of $\Omega^0 = 2.2$ GHz, which corresponds to a wavelength λ^* of about 136.4 mm in free space. For this frequency range the dimensions of the cell are set to $14 \times 20 \times 30$ mm (Fig. 7) ($\lambda/d \approx 9.7$). The back plane is 1 mm thick and made of a lossless dielectric with $\varepsilon_r = 2.2$. The conductive layer is 35 μm thick, made of copper, and is printed on both sides of the plate in anti-symmetric patterns. The patterns are symmetric about the y_1 axis (Fig. 3c). 2 mm spacers are added to the $\pm$ **k** faces of the cell and the input and output surfaces Γ_1 and Γ_2 are taken as the exterior surfaces.

The domain is discretized using linear finite elements. The discretization is graded in the x_1 direction (with smaller elements near the inclusion) but uniform in the (x_2, x_3) plane.

4.1 Example 1: study of local optima and the effect of "gray" pixels

This simple example highlights the presence of local optima and the effect of even a small number of gray pixels on performance. The design domain D is discretized using 14×20 elements, but conductive material can be placed only in the center 10×10 region, symmetrically about the mid plane. Iterations start from a random initial design. $\sigma^L_{dB} = -7$ and a standard filter (Bruns and Tortorelli 2001; Bourdin 2001) with $r_{min} = 2$ are used in stage 1.

The final solution shown in Fig. 8a meets the necessary conditions for optimality (15). This solution has exactly four (independent) gray pixels. Nevertheless, the presence of even this small number of gray pixels has a significant effect on performance. If the gray pixels are removed, the resulting structures (Fig. 8c, d) have very different performance at 2.2 GHz, as shown in Fig. 8e.

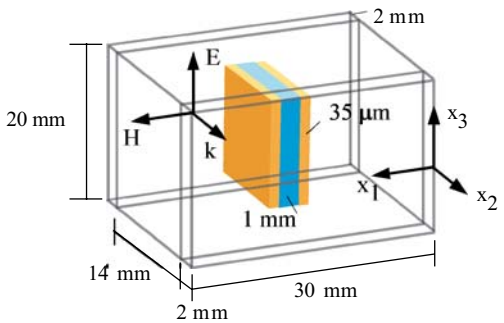

Fig. 7 The representative cell used in examples

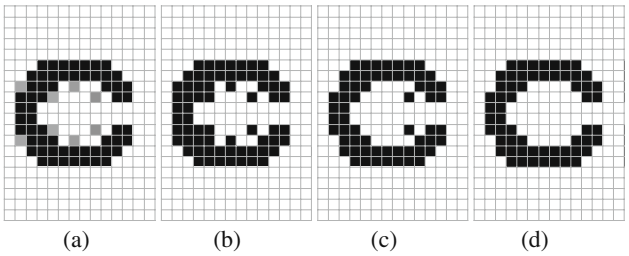

	a	b	c	d
Γ	0.0267	0.00871	0.0086	0.0117
min μ″	−3.87	−14.5	−14.9	−9.73
ω*	2.21	2.31	2.29	2.37

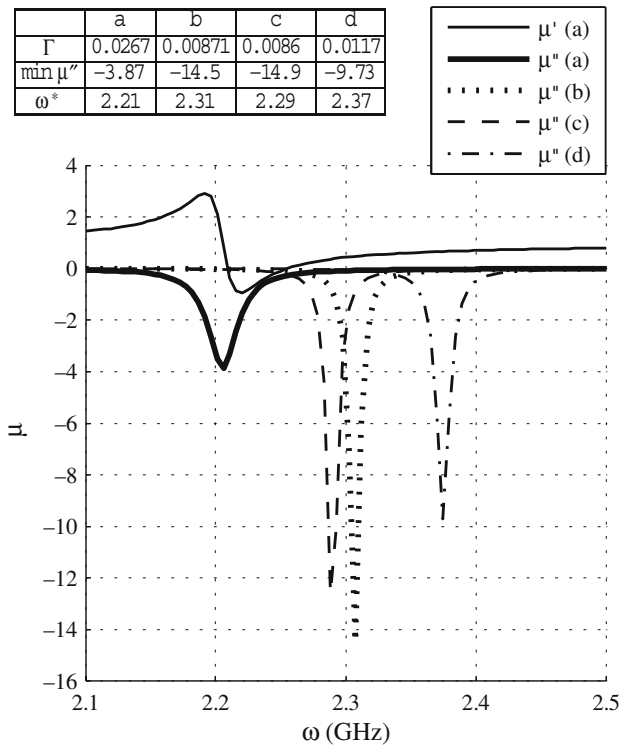

Fig. 8 Possible solutions to Example 1 at $\Omega^0 = 2.2$ GHz. Initial design is random. Solution (**a**) and post-processing using various thresholds (**b**) 0.3, (**c**) 0.5, (**d**) 0.7

The results displayed in Fig. 8 show some interesting features. Most notably, the removal of the gray areas sharpens the strength of the resonance and shifts the frequency of resonance to a higher value. To understand this behavior, one could think of the effective permeability of the system as modeled by a Lorentz-type resonator with parameters F, ω_0 and Γ that depend on the effective density ρ, i.e.,

$$\mu_{eff}(\omega) \approx \mu_L(\omega) = 1 - \frac{F(\rho)\,\omega^2}{\omega^2 - \omega_0(\rho)^2 + j\omega\Gamma(\rho)} \qquad (16)$$

Solutions with gray pixels behave as Lorentz resonators with larger values of Γ in (16) and thus are associated with larger resistance losses and a broader bandwidth but shallower resonance. The functional form of $\mu_L(\omega)$ in (16) in fact matches rather well the numerical results obtained for $\mu_{eff}(\omega)$. Using a best fit estimate, the value of Γ for the gray solution (a) in Fig. 8 is $\Gamma = 0.0267$, while the corresponding values for the binary results (b)–(d) are lower, respectively 0.00864, 0.00871 and 0.0117. Interestingly, the value (d) for binary solution Γ is higher than that of the other two binary answers. This suggests that higher bandwidth may be achieved simply by tailoring the material layout, a result that may be exploited in future work.

The increase in the resonance frequency is harder to explain: in this example, if χ^* is the binary design obtained by thresholding of a local optimum ρ^* of (10), $\omega_0(\chi^*) > \omega_0(\rho^*)$. Essentially, it appears that at least in this example, a sharper contrast always increases the resonance frequency.

It is also noted that at ρ^* associated with solution (a), the minimum value of μ'' over frequency is not achieved at Ω^0, i.e., $\Omega^0 \neq \omega^* = \arg\min_{\omega} \mu''(\omega, \rho^*)$. In fact, equality should

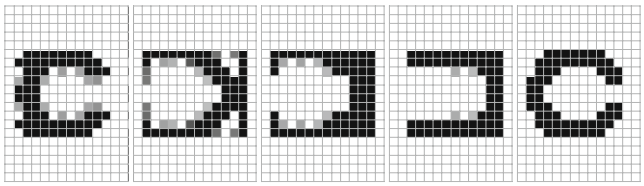

	a	b	c	d	e
Γ	0.0415	0.032	0.0326	0.0256	0.0117
min μ″	−2.6	−3.46	−3.61	−5.32	−9.73

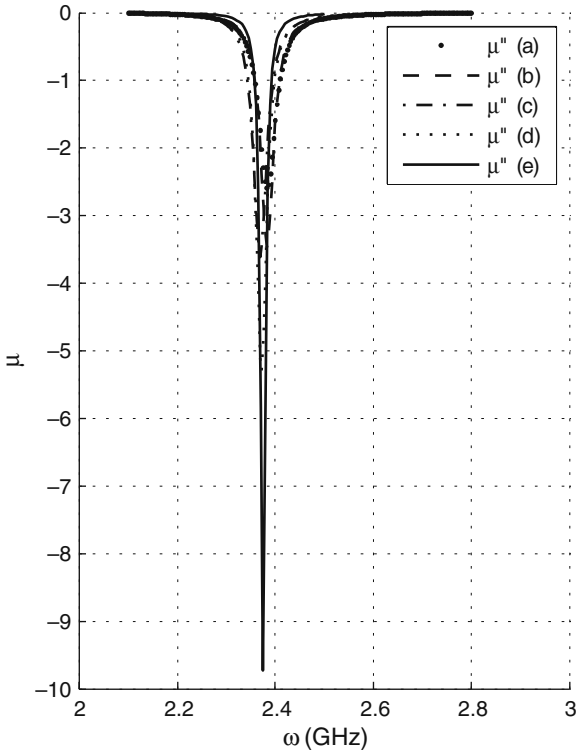

Fig. 9 Locally optimal solutions to Example 1 at $\Omega^0 = 2.375$ GHz

not be expected unless Γ vanishes (and F is constant). Furthermore, unlike the spring analogy in the previous section, in this case one should not expect the "undamped" resonant frequency $\omega_0(\rho^*)$ to match Ω^0 either, since Γ is now design dependent. However, as Γ is a small number around the solution ρ^*, the differences between Ω^0, ω^* and $\omega_0(\rho^*)$ are small.

The binary design (d) in Fig. 8 has a resonance at $\omega = 2.375$ GHz. Since a binary solution is now known to resonate at this frequency, one would expect that if the target frequency were set to this value (i.e., setting $\Omega^0 = 2.375$ GHz) the algorithm should converge to the known binary answer. However, this is by no means guaranteed and depends largely on the initial design. Along with the binary solution, a plethora of other designs that resonate at 2.375 GHz exist, and depending on the initial parameters, the algorithm may converge to any one of them! Some of the possible results for $\Omega^0 = 2.375$ GHz are shown in Fig. 9. All these designs satisfy the first order conditions (15). Note that, as observed before, the amount of gray correlates with the magnitude of Γ in the approximation of μ_{eff} (16), more gray resulting in larger Γ and therefore broader but weaker resonances.

Finally, it should be emphasized that these observations apply only to small changes in densities around an already resonant design made up mostly of binary values.

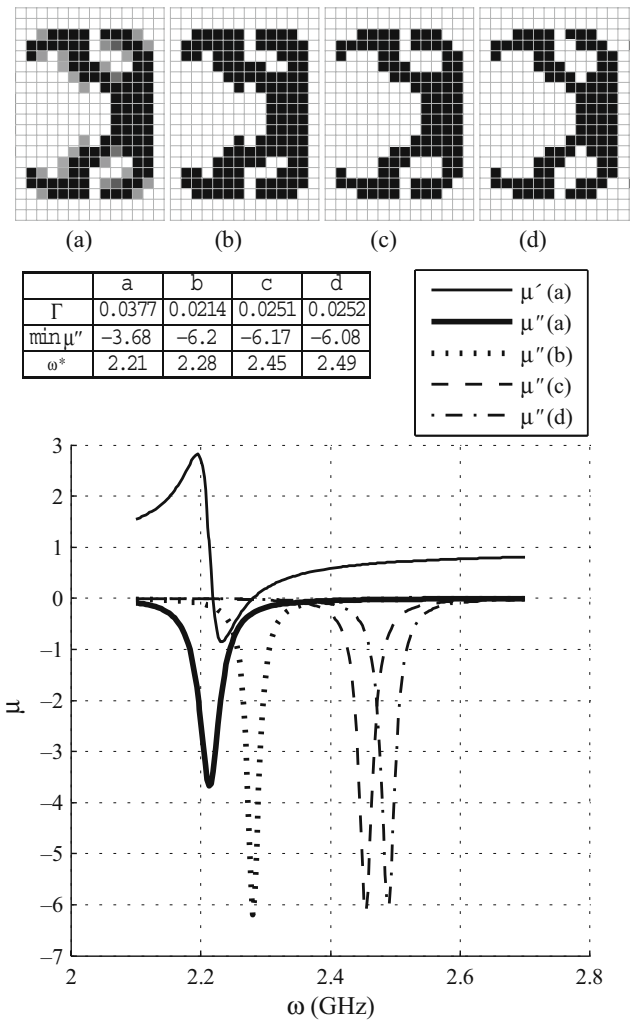

Fig. 10 Possible solutions to Example 2 at $\Omega^0 = 2.2$ GHz. Solution (**a**) and post-processing using various thresholds (**b**) 0.3, (**c**) 0.5, (**d**) 0.7

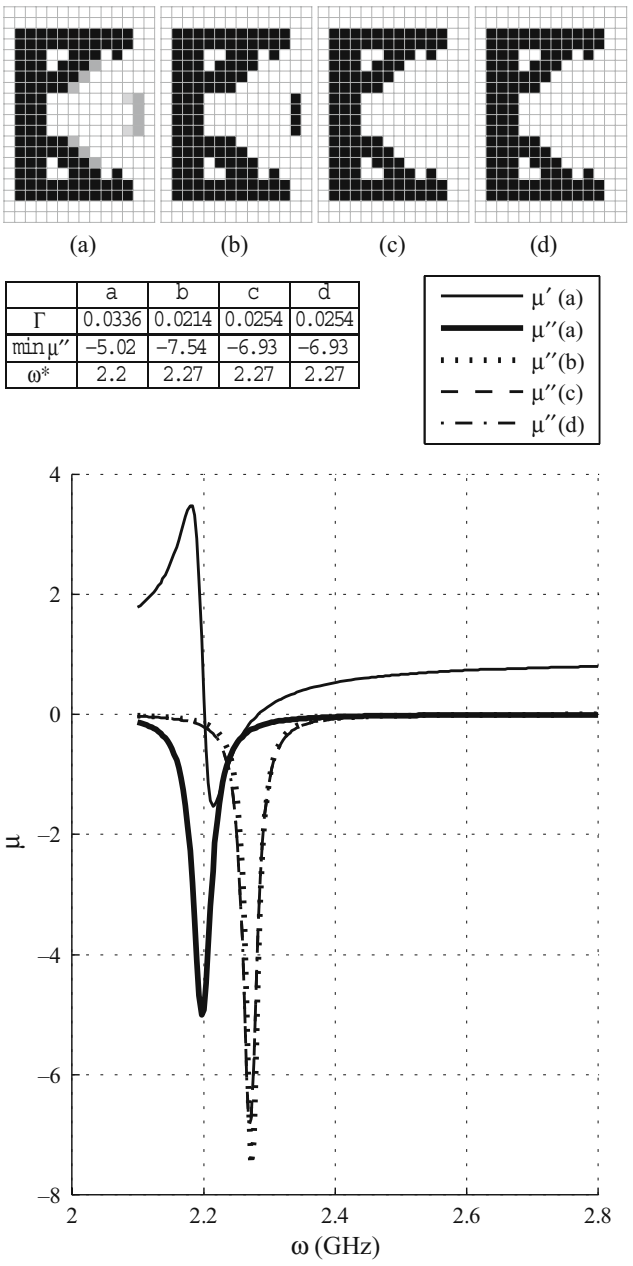

Fig. 11 Alternative solutions to Example 2 at $\Omega^0 = 2.2$ GHz. Initial design is uniform $\rho = 0.5$. Solution (**a**) and post-processing using various thresholds (**b**) 0.3, (**c**) 0.5, (**d**) 0.7

In general, a randomly generated design will not exhibit resonances and no amount of thresholding will make it resonate.

4.2 Example 2

In this example the design domain is enlarged to cover a larger area of the center plate D. The discretization of D is still a coarse 14×20 array and the design domain covers the middle, 12×16 region. $\sigma_{dB}^{L} = -5$ and other parameters are as in the previous example.

Two locally optimal solutions are presented in Figs. 10 and 11. These are obtained for the same target frequency $\Omega^0 = 2.2$ GHz but from two different starting designs. As before, convergence is achieved only to designs with a small number of "gray" pixels, but the effect of these pixels on the solution is significant. In each case, a binary answer is obtained by thresholding of the local optimum, using a simple Heaviside function centered, respectively, at 0.3, 0.5

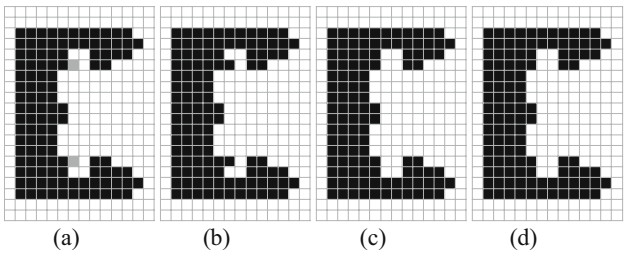

	a	b	c	d
Γ	0.0202	0.0195	0.0175	0.0175
min μ″	−8.4	−8.67	−9.89	−9.89
ω*	2.	2.02	2.02	2.02

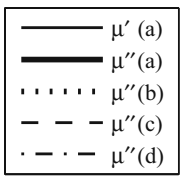

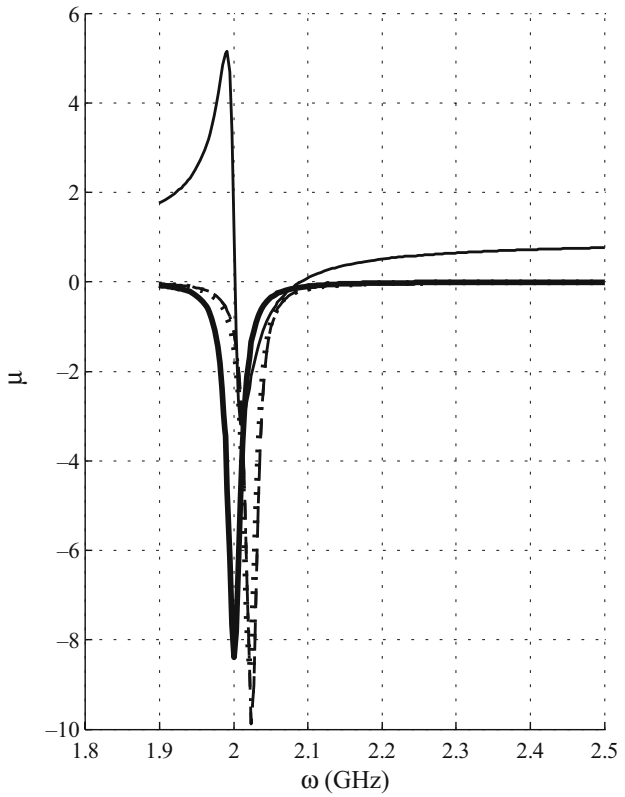

Fig. 12 Possible solutions to Example 2 at $\Omega^0 = 2.0$ GHz. Solution (**a**) and post-processing using various thresholds (**b**) 0.3, (**c**) 0.5, (**d**) 0.7

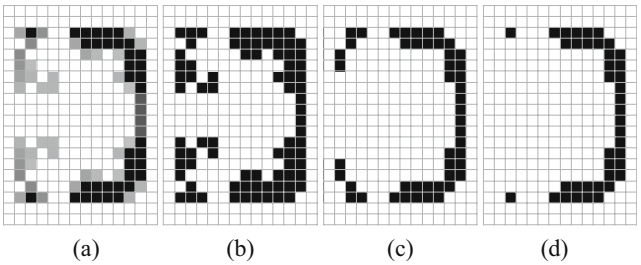

	a	b	c	d
Γ	0.086	0.0731	0.0892	0.0887
min μ″	−4.13	−5.12	−4.73	−4.73
ω*	2.63	2.81	3.02	3.03

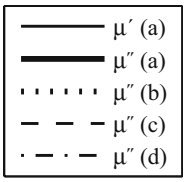

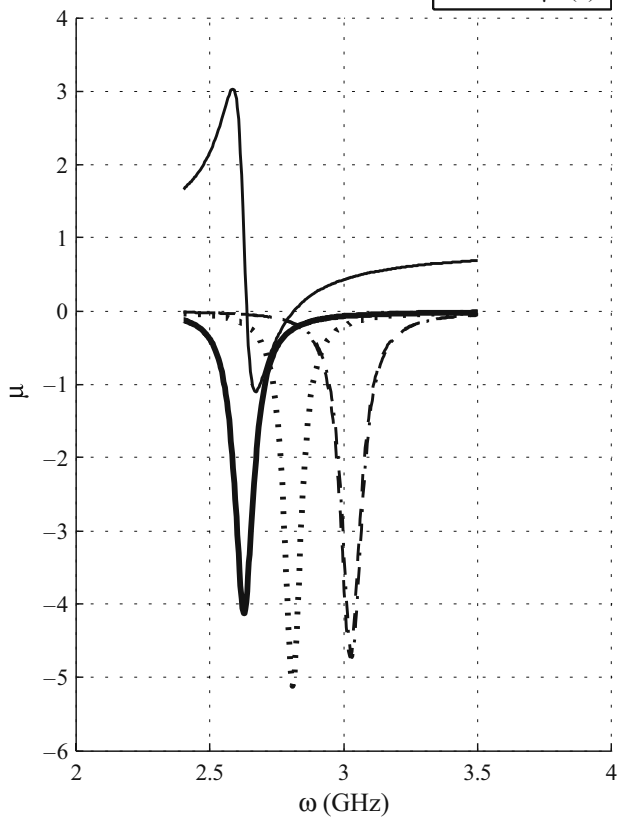

Fig. 13 Possible solutions to Example 2 at $\Omega^0 = 2.6$ GHz. Solution (**a**) and post-processing using various thresholds (**b**) 0.3, (**c**) 0.5, (**d**) 0.7

and 0.7 for figures (b), (c) and (d). Gray regions of low conductivity result in higher damping and broader but shallower resonances. The effect of thresholding is to shift the resonance to a higher frequency, all consistent with the results observed in Example 1.

Figures 12, 13 and 14 show results for different target frequencies Ω^0. The general behavior of the solutions is unchanged from the previous example.

Figure 15 shows the result obtained using a combination of minimization of μ'' and μ' as the objective function

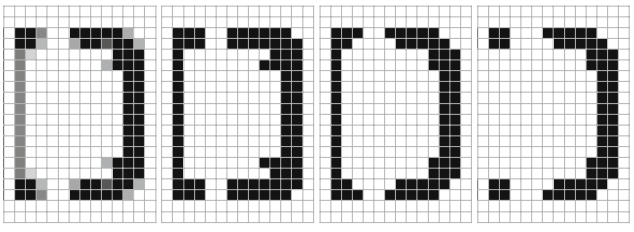

(a) (b) (c) (d)

	a	b	c	d
Γ	0.106	0.0967	0.117	0.107
min μ″	−3.97	−4.49	−4.03	−4.15
ω*	3.03	3.06	3.29	3.31

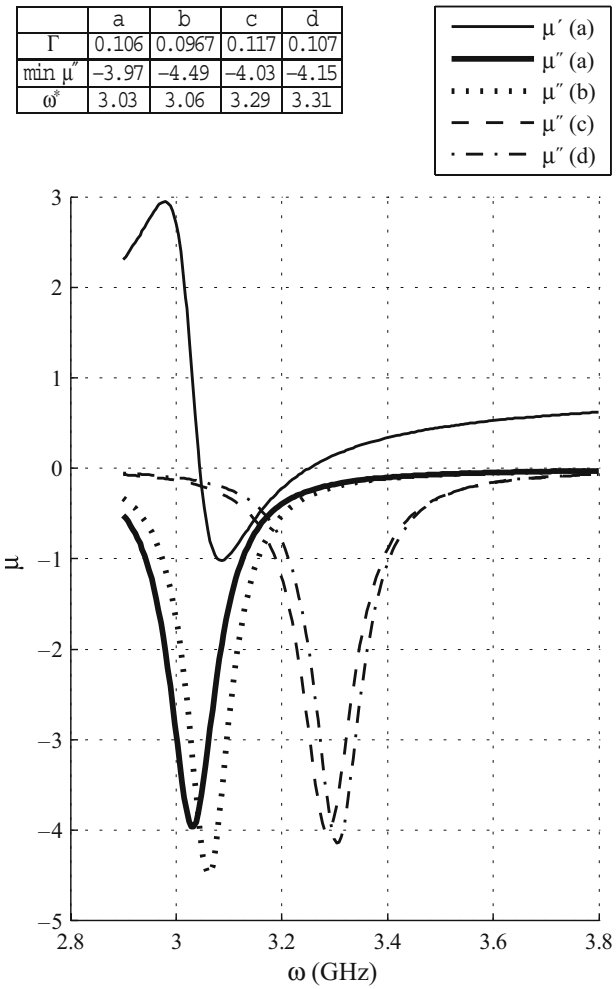

Fig. 14 Possible solutions to Example 2 at $\Omega^0 = 3.0$ GHz. Solution (**a**) and post-processing using various thresholds (**b**) 0.3, (**c**) 0.5, (**d**) 0.7

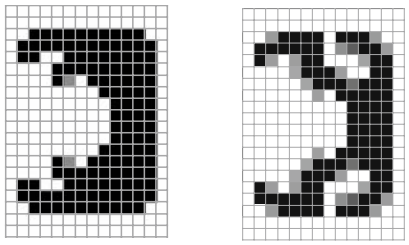

(a) min μ″ followed by min μ′ (b) min μ″

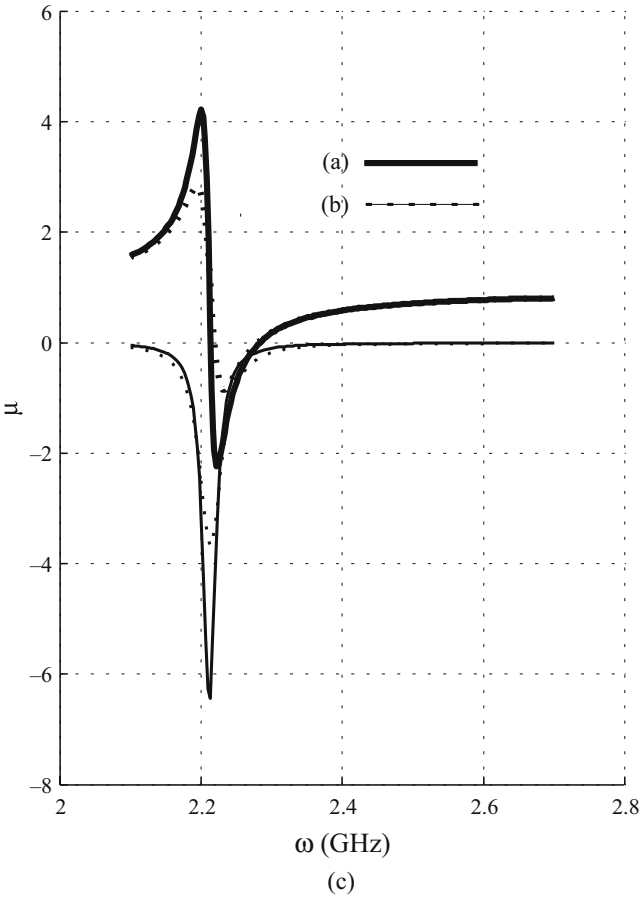

(c)

Fig. 15 Solution to Example 2 using as the objective function: (**a**) a combination of μ'' and μ' and (**b**) μ'' alone. The corresponding effective permeability is shown in (**c**)

and a target frequency of $\Omega^0 = 2.2$ GHz. Minimization of μ'' is applied first, implementing the first stage of the algorithm described in Section 3.6. This step is required to find a suitable starting design from which minimization of μ' can proceed. After an initial design with $\mu''(\Omega^0) < 0$ is found, the algorithm in Section 3.6 can be applied using now μ' as the objective function to be *minimized*. This variation of the problem results in solutions that are qualitatively similar to the results found using μ''. In this example the combined minimization of μ'' and μ' results in a solution with fewer gray pixels and, as a result, a sharper resonance. This is not always the case.

4.3 Example 3

This example is essentially the same as Example 2, but now solved over a refined design space whereby ρ is discretized over a now finer 28×40 grid. Solutions for various target frequencies are shown in Figs. 16, 17, 18, and 19 and, unless noted, they are obtained starting from an initially random design. Other than the obvious increase in computational burden, the new solutions highlights few new features. With a refined mesh newer and more intricate designs become accessible. Intricate designs also have a larger exposed perimeter and therefore the potential for convergence to solutions with larger "gray" areas is greater. However, despite the complexity of some of the geometries found, in all cases only one resonance is found near the target frequency. This is perhaps not surprising in this case, given that our analysis was restricted to a single-cell deep slab and the fact that the cell size is much smaller than the

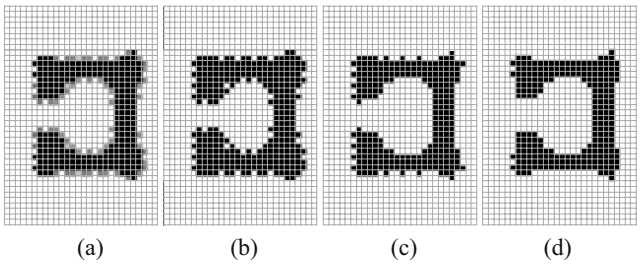

(a) (b) (c) (d)

	a	b	c	d
Γ	0.0204	0.0102	0.0121	0.0144
$\min \mu''$	−4.9	−11.3	−8.71	−7.45
ω^*	2.2	2.34	2.33	2.48

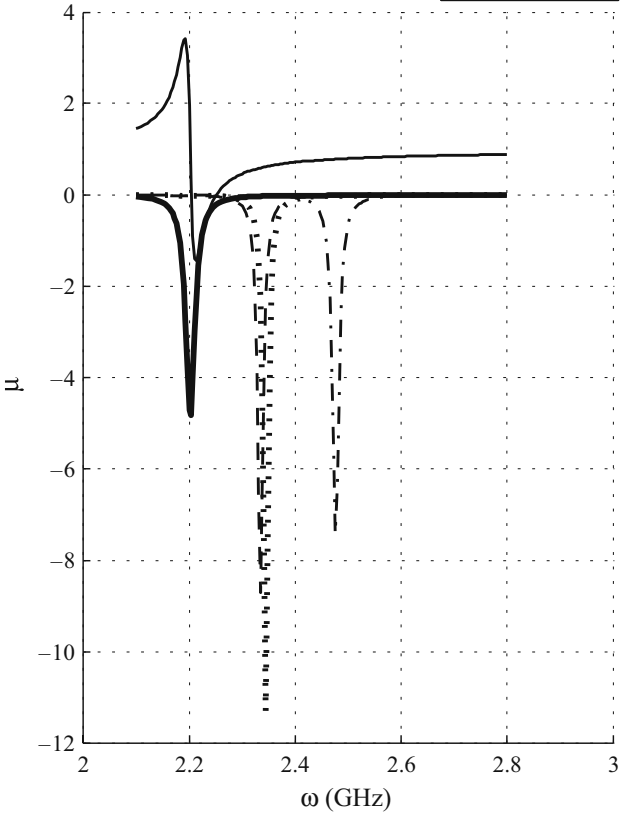

Fig. 16 Possible solutions to Example 3 at $\Omega^0 = 2.2$ GHz. Solution (**a**) and post-processing using various thresholds (**b**) 0.3, (**c**) 0.5, (**d**) 0.7. Design domain is restricted to a 20×20 pixel section of rectangle

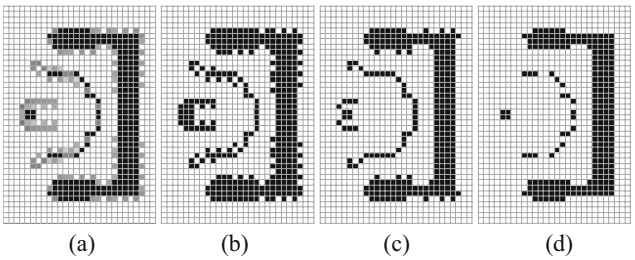

(a) (b) (c) (d)

	a	b	c	d
Γ	0.0441	0.0354	0.0356	0.0412
$\min \mu''$	−5.42	−7.19	−7.24	−6.72
ω^*	2.21	2.31	2.32	2.53

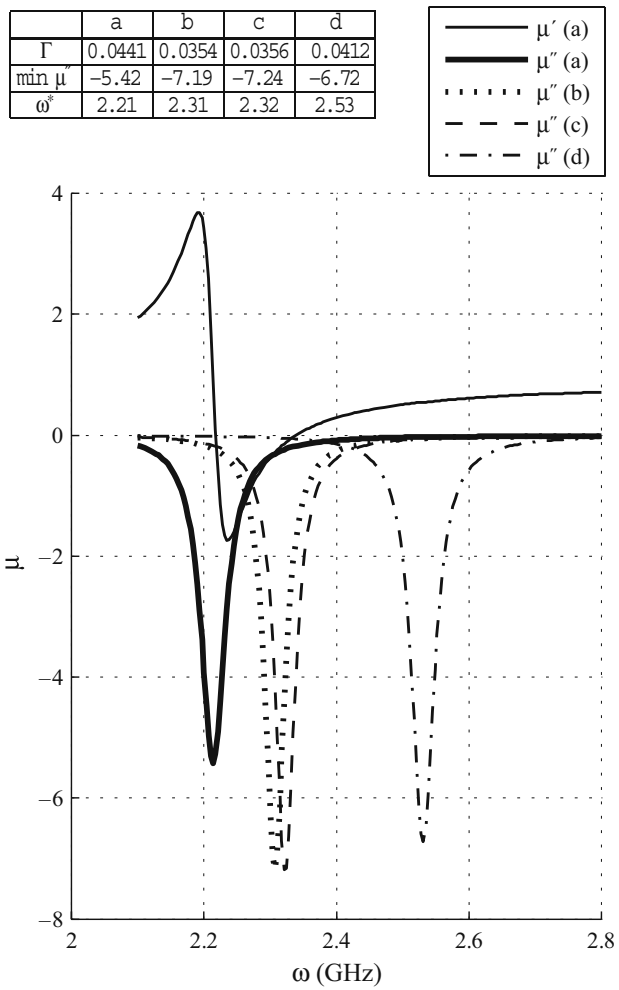

Fig. 17 Possible solutions to Example 3 at $\Omega^0 = 2.2$ GHz. Solution (**a**) and post-processing using various thresholds (**b**) 0.3, (**c**) 0.5, (**d**) 0.7. Initial design is uniform

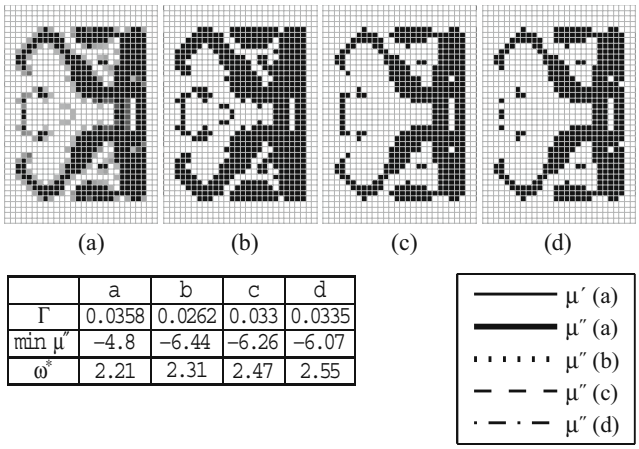

	a	b	c	d
Γ	0.0358	0.0262	0.033	0.0335
min μ″	−4.8	−6.44	−6.26	−6.07
ω*	2.21	2.31	2.47	2.55

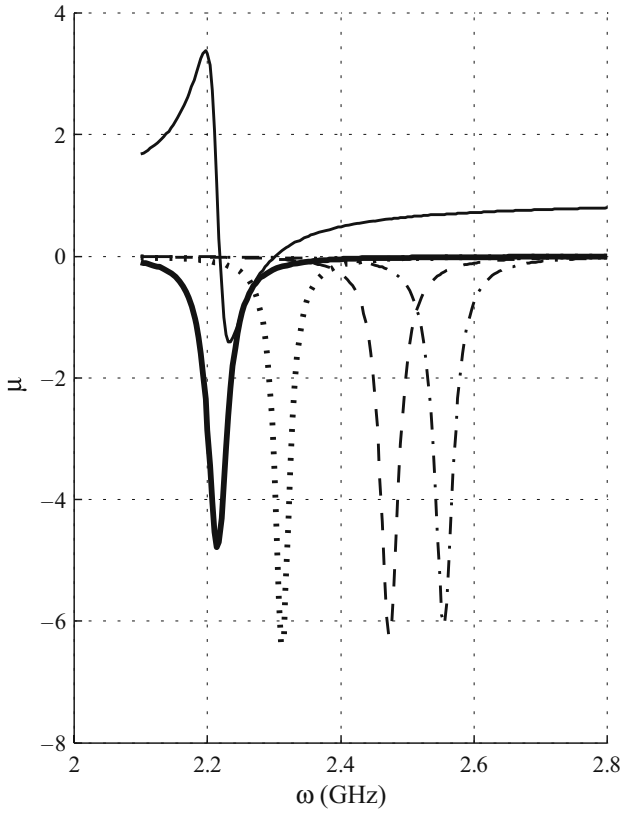

Fig. 18 Possible solutions to Example 3 at $\Omega^0 = 2.2$ GHz. Solution (**a**) and post-processing using various thresholds (**b**) 0.3, (**c**) 0.5, (**d**) 0.7

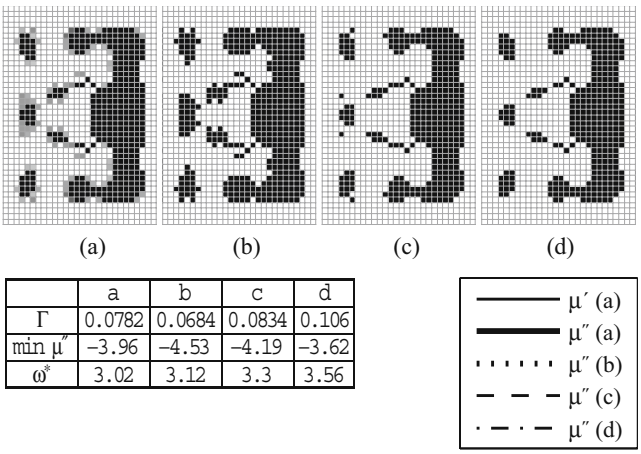

	a	b	c	d
Γ	0.0782	0.0684	0.0834	0.106
min μ″	−3.96	−4.53	−4.19	−3.62
ω*	3.02	3.12	3.3	3.56

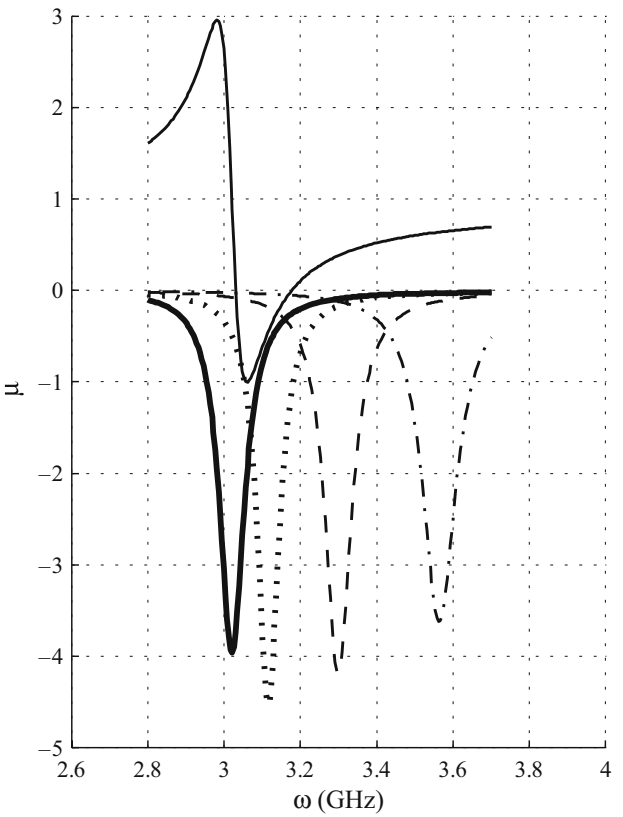

Fig. 19 Possible solutions to Example 3 at $\Omega^0 = 3.0$ GHz. Solution (**a**) and post-processing using various thresholds (**b**) 0.3, (**c**) 0.5, (**d**) 0.7

wavelength. The next eigenmodes occur much farther up the spectrum.

Occasionally, the algorithm results in solutions with unusual checkerboard-like patterns on the boundary, probably numerical artifacts not related to any underlying physics. These patterns may be present even in quadratic finite element models. The mechanism that supports the appearance of these patterns is unclear.

5 Conclusions

The presence of a resonance and its relevance to the performance of the design and the existence of many local optima make the solution of this problem particularly challenging. Traditional filters work to some extent to eliminate gray areas but are unable to remove all gray pixels. For this, a different approach may be needed, perhaps a different filter design or even the use of a hybrid optimization

method capable of handling the integer programming problem at later stages in the design. The analysis is involved and time consuming, and as a result it is unlikely that a method such as a genetic algorithm provide answers in any but the smallest of discretizations. However, a hybrid approach may involve genetic algorithms in the later stages, only to remove the last few remaining gray pixels from the design.

The present approach is sufficient for the present problem, where the interest is only in finding solutions with negative permeability. In this case the frequency shift caused by the post-processing step can be easily adjusted back if scaling of the cell dimensions is allowed, as the resonant frequency scales with cell size. However if a more complex performance function is contemplated—e.g., solutions with negative permeability over a broad spectrum of frequencies—convergence to true binary solutions would be crucial and the algorithm must be refined.

Acknowledgments This material is based upon work supported, in part, by the US National Science Foundation under grant no. 0800388 (ARD) and by the Danish Research Council for Technology and Production Sciences under grant no. 274-06-0507 (OS). This support is gratefully acknowledged.

References

Bendsøe MP (1990) Optimal shape design as a material distribution problem. Struct Optim 1:193–202

Bourdin B (2001) Filters in topology optimization. Int J Numer Methods Eng 50(9):2143–2158

Bruns TE, Tortorelli DA (2001) Topology optimization of non-linear elastic structures and compliant mechanisms. Comput Methods Appl Mech Eng 190(26–27):3443–3459

Guest JK, Prevost JH, Belytschko T (2004) Achieving minimum length scale in topology optimization using nodal design variables and projection functions. Int J Numer Methods Eng 61(2):238–254

Jin J (2002) The finite element method in electromagnetics, 2nd edn. Wiley, New York

Lerat JM, Mallejac N, Acher O (2006) Determination of the effective parameters of a metamaterial by field summation method. J Appl Phys 100(8):084908.1–084908.9

Marqués R, Martin F, Sorolla M (2008) Metamaterials with negative parameters. Wiley-Interscience, New Jersey

Mlejnik HP, Schirrmacher R (1993) An engineering approach to optimal material distribution and shape finding. Comput Methods Appl Mech Eng 106:1–26

Olesen LH, Okkels F, Bruus H (2006) A high-level programming-language implementation of topology optimization applied to steady-state Navier–Stokes flow. Int J Num Methods Eng 65(7): 975–1001

Pendry JB (2000) Negative refraction makes a perfect lens. Phys Rev Lett 85:3966–3969

Pendry JB, Holden AJ, Robbins DJ, Stewart WJ (1999) Magnetism from conductors and enhanced nonlinear phenomena. IEEE Trans Microwave Theor Tech 47(11):2075–2084

Rockstuhl C, Paul T, Lederer F, Pertsch T, Zentgraf T, Meyrath TP, Giessen G (2008) Transition from thin-film to bulk properties of metamaterials. Phys Rev, B 77:035126. doi:101103/PhysRevB77035126

Rozvany GIN, Zhou M, Birker T (1992) Generalized shape optimization without homogenization. Struct Optim 4:250–254

Schelkunoff SA, Friis HT (1952) Antennas: the theory and practice. Wiley, New York, pp 584–585

Sigmund O (2007) Morphology-based black and white filters for topology optimization. Struct Multidiscipl Optim 33(4–5):401–424

Smith DR, Pendry JB (2006) Homogenization of metamaterials by field averaging. J Opt Soc Am B 23(3):391–403

Smith DR, Padilla WJ, Vier DC, Nemat-Nasser SC, Schultz S (2000) A composite medium with simultaneously negative permeability and permittivity. Phys Rev Lett 84:4184–4187

Smith DR, Vier DC, Koschny, Soukoulis CM (2005) Electromagnetic parameter retrieval from inhomogeneous metamaterials. Phys Rev E 71, paper no. 036617

Svanberg K (1987) The method of moving asymptotes. Int J Numer Methods Eng 24:359–373

Veselago VG (1968) The electrodynamics of substances with simultaneously negative values of “epsilon” and “mu”. Sov Phys Usp 10(4):509–514